

Simulation of counterflow pedestrian dynamics using spheropolygons

Fernando Alonso-Marroquín,^{*} Jonathan Busch, and Coraline Chiew
School of Civil Engineering, The University of Sydney, Sydney, NSW, Australia

Celia Lozano[†]

Departamento de Física, Facultad de Ciencias, Universidad de Navarra, 31080 Pamplona, Spain

Álvaro Ramírez-Gómez

Departamento de Ingeniería Mecánica, Química y Diseño Industrial, Universidad Politécnica de Madrid, Spain

(Received 19 November 2013; revised manuscript received 16 October 2014; published 8 December 2014)

Pedestrian dynamic models are typically designed for comfortable walking or slightly congested conditions and typically use a single disk or combination of three disks for the shape of a pedestrian. Under crowd conditions, a more accurate pedestrian shape has advantages over the traditional single or three-disks model. We developed a method for simulating pedestrian dynamics in a large dense crowd of spheropolygons adapted to the cross section of the chest and arms of a pedestrian. Our numerical model calculates pedestrian motion from Newton's second law, taking into account viscoelastic contact forces, contact friction, and ground-reaction forces. Ground-reaction torque was taken to arise solely from the pedestrians' orientation toward their preferred destination. Simulations of counterflow pedestrian dynamics in corridors were used to gain insight into a tragic incident at the Madrid Arena pavilion in Spain, where five girls were crushed to death. The incident took place at a Halloween Celebration in 2012, in a long, densely crowded hallway used as entrance and exit at the same time. Our simulations reconstruct the mechanism of clogging in the hallway. The hypothetical case of a total evacuation order was also investigated. The results highlight the importance of the pedestrians' density and the effect of counterflow in the onset of avalanches and clogging and provides an estimation of the number of injuries based on a calculation of the contact-force network between the pedestrians.

DOI: [10.1103/PhysRevE.90.063305](https://doi.org/10.1103/PhysRevE.90.063305)

PACS number(s): 45.70.Mg, 64.60.av, 89.65.-s

I. INTRODUCTION

Pedestrian dynamics modeling has been a subject of mathematical investigation since the 1950s [1,2] and was originally used by Hankin and Wright to study the movements of pedestrians in the London subway to allow for more efficient design of stairs and corners. The study of pedestrian panic, however, began later in the 1970s [3] in response to several of history's most horrific crowd stampedes. The most notable of these occurred in Chongqing, China, during World War II. On 6 June 1941 an air raid shelter was evacuated following a Japanese raid and approximately 4000 people were killed in a resulting panic-driven stampede. The majority of fatalities were due to asphyxiation [4]. The sites where the Muslim pilgrimage, or Hajj, converges on Mecca have a long history of deaths due to pedestrian panics. When pilgrim luggage spilled over Mecca's narrow Jamarat Bridge in 2006, the crowd was sent into panic; at least 345 people were killed, and 289 were injured [5].

Every year hundreds of people are hurt or lost in crowd disasters. Since Helbing *et al.* [6] published on intermittent flow and clogging in evacuation processes in 2000, there have been many publications modeling pedestrian behavior: cellular automata models, [7–10], game theory models [11–13], and mechanistic models [14]. These models address different aspects such as counterflow conditions [7,8,15], transitions

from laminar to stop-and-go and *turbulent* flows [5,16], as well as the effects of competition and cooperation of pedestrians [10,17].

A number of studies have considered the clogging events in animals [18,19], traffic flows [20], or granular flow [21,22]. Despite the different nature in all these cases, we observe similarities in the collective behavior. Strategies to control clogging, such as achieving lower terminal velocities by reducing panic [23] or placing an obstacle before the exit to reduce the pressure and the density at the bottleneck [24,25], are common across a number of studies. Our aim is to formulate a mechanistic, granular dynamics-based model for pedestrian dynamics and to identify in which extend this model can be used for advance warning of crowd disasters: the importance of the pedestrian shape, density, and counterflow.

Over the past 2 decades, the key challenge in pedestrian dynamic modeling has been to describe rules that guide how the agents (considered as particles in many cases) interact with each other in a way that faithfully reproduces behaviors. Earlier studies suggested that pedestrians can be described as reacting to a social force, which dictates the direction and acceleration [14]. The social-force model of Helbing and Molnar is one of the best-known approaches to simulate pedestrian motion, a collective phenomenon with nonlinear dynamics. The social-force model considers that the Newtonian laws of motion mostly carry over to pedestrian motion. Therefore, human trajectories can be computed solving a set of ordinary differential equations for velocity and position.

Our model takes special care of cross-sectional pedestrian shape, contact forces between pedestrians, and ground-reaction forces of torques. We use this method to study of

^{*}fernando.alonso@sydney.edu.au

[†]Present address: Physikalisches Institut, Universität Stuttgart, Pfaffenwaldring 57, 70569 Stuttgart, Germany; Max-Planck-Institut für Intelligente Systeme, Heisenbergstraße 3, 70569 Stuttgart, Germany.

pedestrian dynamics under crowd condition to shed light on a well-documented, tragic incident in Spain on 31 October 2012 at the Madrid Arena pavilion. The venue was already highly overcrowded when more people entered, and security personnel failed to control the distribution of the crowd, leading to the crushing death of five teenagers when the passageway to the central court was blocked.

This paper is organized as follows. Section II describes the spheropolygon-based model used to perform the simulations; Sec. III describes the Madrid Arena venue and the particular circumstances preceding the tragic incident; Sec. IV includes the results of simulations in the hallways where the fatalities happened. We also calculate the cumulative distribution of contact forces in the hallway and compare it with the distribution in the case of evacuation of the whole venue. Conclusions and discussion of our results are presented in Sec. V.

II. FORMULATION OF THE PEDESTRIAN DYNAMICS MODEL

The numerical study conducted in this paper is based on a contact-force model for pedestrians. The force equations are implemented in a spheropolygon-based model previously used to simulate granular materials [26–28]. The advantage of the spheropolygons is that the contact forces among them can be efficiently calculated from their vertex-edge distances, as is explained in detail in Ref. [26]. As well as these contact forces, our model includes ground-reaction forces and torques that reflect the desired motion of the pedestrians and their response to the crowd movement.

A. Shape representation

Nonspherical shapes have been considered in the pursuit of an increasingly accurate description of pedestrian mechanics [29–32]. In catastrophes involving high densities, the packing arrangement of pedestrians more closely reflects the cross-sectional design of the chest and arms rather than the head. The head has a degree of flexibility, in that it can rotate to avoid collisions, and can fit, from an overhead view, within the area of the thorax and arms. This is consistent with a review conducted from publicly available footage of pedestrian disasters [31,32].

To obtain a more accurate pedestrian shape, a chest cross section of a human thorax, including the arms was obtained from the U.S. National Library of Medicine [33], is represented by the concept of Minkowski’s sum of a polygon with a disk (see Fig. 1). This permits the representation of complex shapes without the need to define the object as a composite of spherical particles. This was recolored to isolate the surface.

Figure 1(a) shows the processed black-and-white image of a thorax, with all pixels inside the thorax black and all others white. The thorax is then represented using a spheropolygon, which is the figure resulting from sweeping a disk into a polygon, seen in Fig. 1(b). To obtain the optimal spheropolygon representing the thorax, we produce a black-and-white image of the test spheropolygon of the same size of the thorax image, where points inside the spheropolygons are black and the others are white. We define the *difference* between the images as the number of pixels whose values between both images

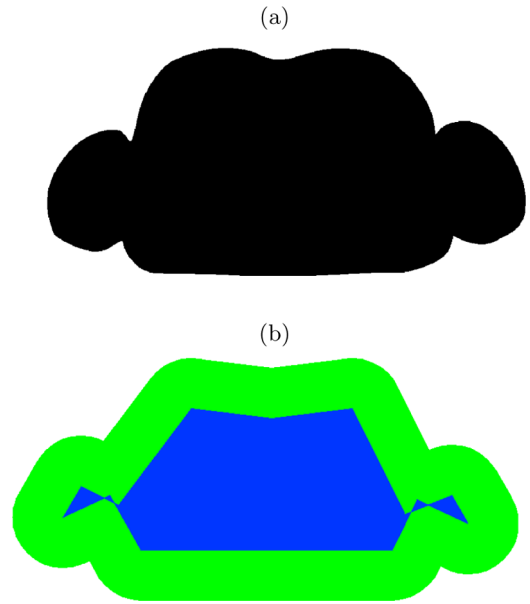


FIG. 1. (Color online) (a) Boundary of the cross-section of a chest derived from a U.S. National Library image of a thorax. (b) Minkowski’s thorax representation by using a spheropolygon with 14 vertices (blue) and a spheroradius of 0.05 m (green).

differ. Based on this difference, an optimization algorithm is used to find the best image by iteratively changing the position of the spheropolygon vertices. The basic idea of this algorithm is to move each vertex in each interaction in the direction opposite to the gradient of the difference between the images. Details of the algorithm can be found in Refs. [34,35]. At the end the image was scaled to reflect a typical sternum dimensions of $200 \times 460 \text{ mm}^2$. The walls are also represented as spherorectangles with 5-cm radius.

B. Force model

The velocity v_i of the pedestrian i can be determined according to Newton’s second law,

$$\vec{F}_i = m_i \frac{d\vec{v}_i}{dt}, \tag{1}$$

where t is the time, m_i is the mass of the pedestrian, and F_i is the force acting on the pedestrian, derived as shown in Eq. (2):

$$\vec{F}_i = \vec{F}_i^0 + \vec{F}_i^b + \sum_c \vec{F}_{ij}^c. \tag{2}$$

The first two terms are ground-reaction forces exerted on the pedestrians by the floor, and the third one $\sum_c \vec{F}_{ij}^c$ is the sum of contact forces produced by other pedestrians and walls.

The first term, \vec{F}_i^0 , denotes the self-driven component of a pedestrian’s motion [6]:

$$\vec{F}_i^0 = \frac{m_i}{\tau} (v_0 \vec{e}_i - \vec{v}_i) \tag{3}$$

Here τ is the time required by the pedestrian to reach the maximal velocity and v_0 the desired speed. The unit vector \vec{e}_i is the desired direction of motion of the pedestrian.

The third term in Eq. (2) is the sum of all interactions with other pedestrians or walls. A *contact* between two particles (pedestrian-to-pedestrian or pedestrian-to-wall) is considered to occur when the distance between one of the vertices of the first particle and the edge of the second one is lower than the sum of the radii of the spheres, see Ref. [26]. Each interaction force of the contact c between particles i and j is calculated as

$$\vec{F}_{ij}^c = \vec{F}_{ij}^{e,n} + \vec{F}_{ij}^{e,t} + \vec{F}_{ij}^{v,n} + \vec{F}_{ij}^{v,t}, \quad (4)$$

where the elastic forces are given by

$$\vec{F}_{ij}^{e,n} = -k_n \delta_{ij}^n \vec{n}_{ij}, \quad (5)$$

$$\vec{F}_{ij}^{e,t} = -k_t \delta_{ij}^t \vec{t}_{ij}, \quad (6)$$

and \vec{n}_{ij} and \vec{t}_{ij} are the normal and tangential unit vectors. The scalar δ_{ij}^n is the overlapping length and denotes the vertex-to-edge distance between the two particles. The scalar denoted by δ_{ij}^t accounts for the tangential elastic displacement given by the frictional force and satisfies the sliding condition by $|F_{ij}^{e,t}| \leq \mu F_{ij}^{e,n}$, where μ is the coefficient of friction. Here k_n and k_t denote the normal and tangential coefficients of stiffness. The last two terms on the right side of Eq. (4) account for the coefficient of restitution between pedestrians [28], which are shown in Eqs. (7) and (8):

$$\vec{F}_{ij}^{v,n} = -m_{ij} \gamma_n v_{ij}^n \vec{n}_{ij}, \quad (7)$$

$$\vec{F}_{ij}^{v,t} = -m_{ij} \gamma_t v_{ij}^t \vec{t}_{ij}, \quad (8)$$

where m_i is the mass of one particle:

$$m_i = \rho A_i \quad (9)$$

and m_{ij} is the effective mass of the two particles in contact:

$$m_{ij} = \frac{m_i m_j}{m_i + m_j}. \quad (10)$$

The density is indicated by ρ , and A_i denotes the area of the two-dimensional particle. The normal and tangential coefficients of damping are respectively given by γ_n and γ_t ; v_{ij}^n and v_{ij}^t denote the normal and tangential components of the contact velocity.

Additionally, \vec{F}_i^b in Eq. (2) is the *back force* acting on each pedestrian. This force captures the avoidance behavior between pedestrians, when pedestrians alter their direction to avoid collision with oncoming pedestrians. It is a ground-reaction force, with two components: One is related to the intention of the pedestrians to step to their right to avoid collision, and its direction is the cross product $\vec{e} \times \vec{k}$, where \vec{k} is the unit vector normal to the floor. The second component is a top-up force in the desired direction \vec{e} . This force is related to the resistance of the pedestrians to being pushed backwards by the crowd. In situations when alcohol and crowded hallways may be involved, this back force will be larger than would be observed in normal social conditions.

The back force is important, because it is responsible for stream formation, which is an attribute of crowd dynamics both in social and panic situations. Equation (11) describes

the back force:

$$\vec{F}_i^b = \Theta(-\vec{e}_i \cdot \vec{v}_i) \frac{m_i v_0}{\tau} \{\Gamma_F \vec{e}_i + \Gamma_L \vec{e}_i \times \vec{k}\}, \quad (11)$$

where the Heaviside step function $\Theta(x)$ returns 1 if $x > 0$ and zero otherwise. This function activates the back force only when the pedestrians are pushed back from their desired direction. The two parameters of the back force are Γ_L , which measures the natural reflex of the people to move right to avoid collision. Γ_F takes into account the human instinct to push forwards if they are pushed back by others. This factor can be considered as a measure of aggressiveness between the pedestrians that we want to quantify in our model.

C. Torque

The methods proposed by Korhonen *et al.* [29,30] and Langston *et al.* [32] will be used as a foundation for refining the rotational equations of motion. The ground-reaction torque accounts for the pedestrian's desire to face toward their preferred destination, as from Ref. [29]. Within the torque which acts on the pedestrian, there is a torque corresponding to the direction of motion, called motive torque, T_i^m , and a damping component T_i^v .

The motive torque is applied by the legs, and they allow the pedestrian to rotate in the direction of desired motion. As such, the torque arising from this movement is given by Ref. [33], which is a disambiguation of the model constant of the approaches used by Langston *et al.* [32] and Korhonen *et al.* [29,30]. The λ term in Eq. (12) is a dimensionless constant that is derived experimentally, $\theta_i^D = \angle(\vec{v}_i)$ represents the angle to the walking direction, and θ_i is the pedestrian's orientation,

$$T_i^m = \frac{\lambda I_i^z}{\tau^2} \left[1 - \exp\left(-\frac{v_i}{v_0}\right) \right] (\theta_i - \theta_i^D). \quad (12)$$

The exponential function is used to take into account lower motive torque at lower speeds. This is a reflection of the fact that pedestrians can freely rotate if their velocity is low.

The damping component of the torque reflects the pedestrians' desire not to rotate if the desired direction does not change. Using a similar framework to Helbing's self-driven force model [6], in which a desired walking velocity determines the final speed of the pedestrian, a desired angular velocity was created. As the pedestrian prefers not to rotate, the desired angular velocity was set at zero. As a consequence, the pedestrian comes to a comfortable stop after a collision rather than continuing to spin. Equation (13) describes this damping force, where τ is the relaxation time of rotation and I_i^z is the moment of inertia:

$$T_i^v = -\lambda \frac{I_i^z}{\tau} \omega_i. \quad (13)$$

The net torque acting at time t on pedestrian i is therefore as described in Eq. (14):

$$\vec{T}_i = \vec{T}_i^m + \vec{T}_i^v + \sum_{j>i} \vec{l}_{ij} \times \vec{F}_{ij}^c. \quad (14)$$

The last term in this equation, \vec{F}_{ij}^c , is the torque produced by the contact forces. The term \vec{l}_{ij} is the *branch vector* connecting the

TABLE I. Summary of the model parameters.

Parameter	Units	Parameter name	Value	Comment
k_n	N/m	Normal stiffness	1×10^5	Calculated from force-displacement relations
k_t	N/m	Tangential stiffness	1×10^4	Estimated from Poisson's ratio of bulk granular materials
μ	Dimensionless	Coefficient of friction	0.4	Obtained from tables of friction between clothes
ε	Dimensionless	Coefficient of restitution	0.4	Estimated based on observations of collisions
λ	Dimensionless	Torsion stiffness	27	Fitted from comparison of simulation with video footage
Γ_F	Dimensionless	Back force parameter	1.0	Fitted from comparison of simulation with video footage
Γ_L	Dimensionless	Lateral force parameter	1.0	Fitted from comparison of simulation with video footage

center of mass of the pedestrian with the point of application of the contact force.

D. Contact parameters

The parameters of the contact-force model were chosen as follows: the thorax responses to forces $k_n = 10^5$ N/m are taken from medical data on thorax deformation [33]; $k_t = 10^4$ N/m leads to a bulk Poisson ratio of 0.3; $\mu = 0.4$ is close to the coefficient of friction between pieces of cloth fabric. The damping parameter $\gamma_n = 10$ s⁻¹ was chosen using the formula of the coefficient of restitution [28] between colliding particles, shown in Eq. (15),

$$\varepsilon = \exp\left(-\frac{\pi \gamma_n / 2}{\sqrt{k_n / m_{ij} - \gamma^2 / 4}}\right). \quad (15)$$

Since not much information is available regarding the coefficient of restitution between pedestrians, we estimated these parameters from video footage of collisions between pedestrians. By measuring the velocities before and after impact, and neglecting the particle rotation after collision, we obtained coefficients of restitution within the range 0.1–0.5. Details of methods to establish the coefficient of restitution from velocities can be found in the literature on granular media [28].

In the model, a coefficient of restitution of $\varepsilon = 0.3$ was used, which allowed the calculation of the damping parameter γ_n from Eq. (7). The reaction time $\tau = 2/3$ s was used, and the terminal velocity v_0 was randomly chosen between 0.8 and 1.2 m/s. The surface density of the pedestrians is $\rho = 10^3$ Kg/m²; mass of the pedestrians was uniformly distributed in the range 40–70 kg. A summary of the key model parameters is provided in Table I.

E. Numerical solution of the equation of motion

The in-house object-oriented computer program SPOLY was used to conduct the simulations. spoly simulates the pedestrian dynamics based on spheropolygons and a five-order predictor-corrector numerical integration [26]. The use of a neighbor table and Verlet distances allows real-time simulation of long hallways with up to 400 pedestrians if simulated as disks. For

spheropolygon the simulations took 10 times longer. For large-scale simulations with around 10 000 pedestrians the algorithm executes around 1 min of simulations per hour. Details relating to the SPOLY code are found in Refs. [27,28].

III. EMPIRICAL OBSERVATIONS

The insights of this study into crowd behavior are important for the organization of safer mass events as the Halloween party in the Madrid Arena pavilion. This is an indoor arena located in Madrid, Spain. It is distributed on three floors (access, intermediate, and low). The ground floor is the main dance floor, and its dimensions are 55×35 m²; see Fig. 2(a).

We recreate the Madrid Arena venue in order to set the scene. The main problem was that the party's organizers were allowed to sell 9000 tickets, but many more people entered, the judge finding that 19 000 tickets had been issued. Investigation estimated that during the Halloween party the number of the attendees on the ground floor was well above 7700, this corresponds to a density higher than four people per square meter.

Official investigation reported a stampede in the main hallway (dimension 12×3 m²) that connected the main dance floor to another area [Fig. 2(a)]. Prior to the stampede, when the performance of the invited artist started, the ground floor was packed, and entry to the venue constrained, see Fig. 2(b). At the time of the incident, the hallway in Fig. 2(a) was used by patrons trying to leave the concert at the same time as patrons trying to enter the main dance floor. This counterflow, in conjunction with high densities of people, triggered avalanches along the hallway. Five avalanches were detected by the security cameras at the end of the corridor one hour before the fatal incident. The last avalanche ended up with people falling down, clogging the hallway for several minutes and causing the death of five girls by crushing and asphyxiation (Fig. 3). The incident was characterized by physical violence, chaos, inability to move in any direction, rising temperatures, claustrophobia, screams, and waning oxygen. In the semidarkness, people were unable to see what lay in front or behind. Some found themselves lifted off the ground, supported by elbows against their ribs. Those of smaller build, particularly girls, were drawn down under

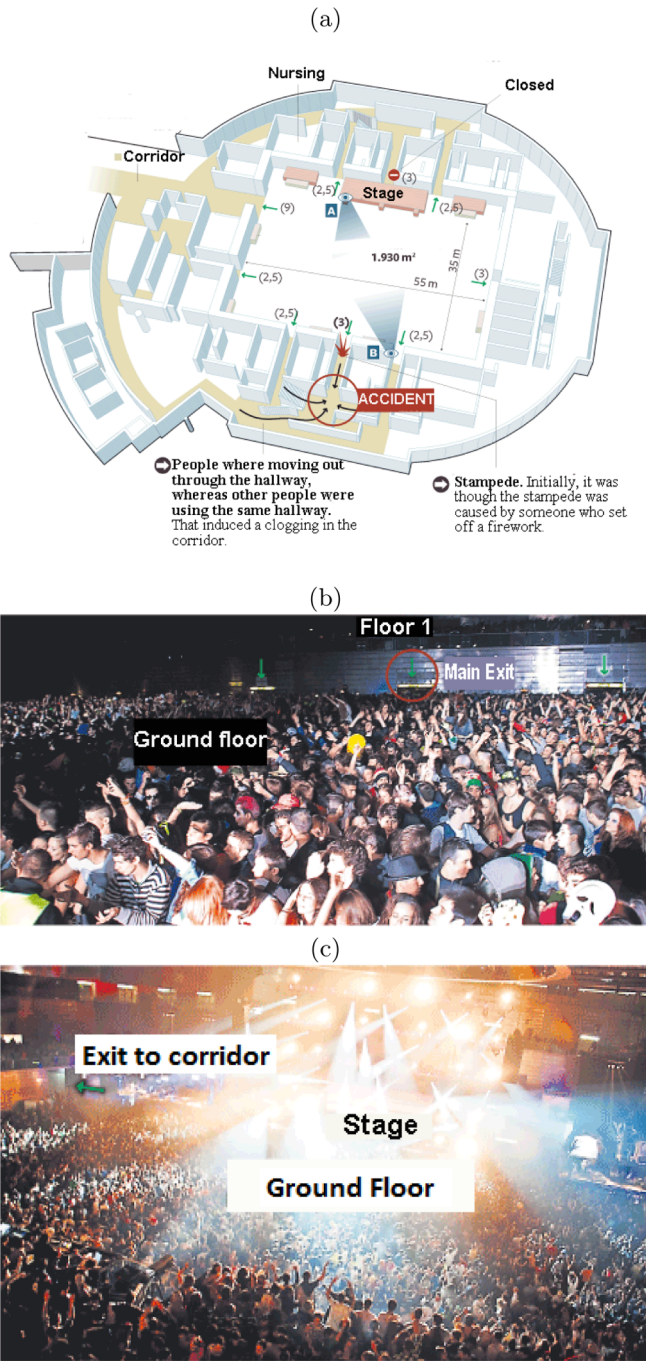


FIG. 2. (Color online) (a) Sketch of the Madrid Arena pavilion. Details of the ground floor of the Madrid Arena marked two points of view A and B of the ground floor. (b) View A shows the entrance of the hallway where the incident happened (red circle). (c) View B shows the ground floor, the main exit, and the position of the stage.

the crush of bodies. Autopsies on the five deceased found suffocation and consequent brain damage as causes of death.

IV. RESULTS

Our model was based on information about crowd density and counterflow taken from video footage and the available

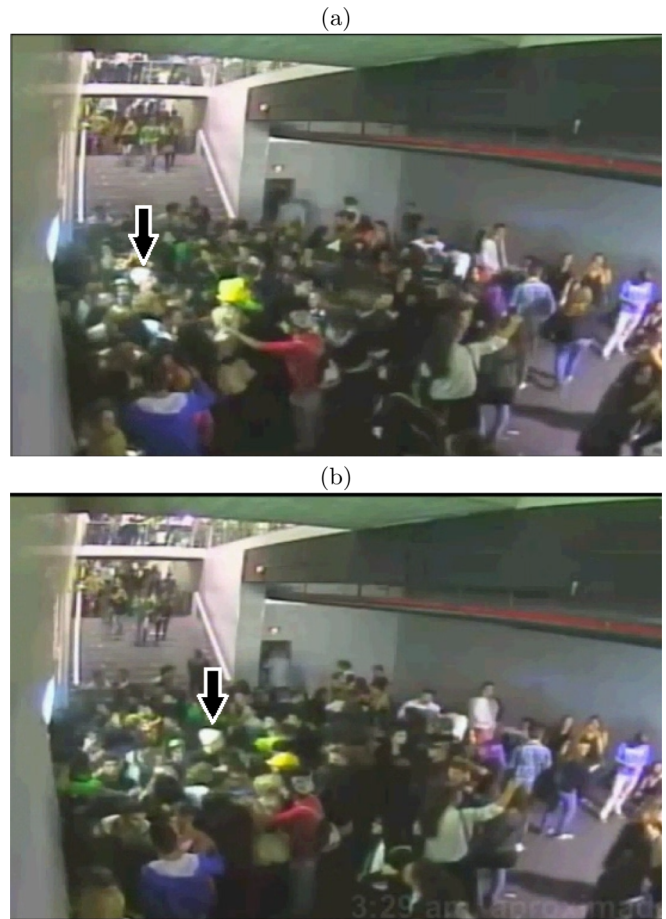


FIG. 3. (Color online) Two snapshots from the video footage showing five dangerous avalanches in Madrid Arena preceding the fatal one. These snapshots are of the fifth avalanche, at end of the corridor. The arrow shows a person with a white hat who we use as tracer. The interval between these snapshots is 0.2 s, suggesting pedestrian velocities up to 3 m/s. Video footage shows increasing density with time in the hallways. The first avalanches happened at 2:18 a.m., 2:29 a.m., 2:41 a.m., 2:59 a.m., and 3:29 a.m. In the fatal incident, registered at 3:33 a.m., people fell down, clogging the hallway.

plans of the Madrid Arena venue. We simulated the main hallway with agents attempting to travel in opposite directions. For each set of parameters, we conducted sensitivity testing with prepared 10 random samples. The total time of simulation was 4 min. The random variables were the desired velocity of the pedestrians v_0 and their mass m . We choose uniformly distributed variables between $v_0 = 0.8-1.2$ m/s and $m = 40-70$ kg. We note that the density of the pedestrian is kept constant and the mass is varied by taking different speropolygon areas. Depending on the crowd density and the ratio of counterflow, we found three different scenarios: lane formation, avalanches, and clogging. A lane formation is the development of two or more coherently moving linear structures [see Fig. 4(a)] that is accompanied by smooth flow where there are almost no collisions among pedestrians. An avalanche is a sudden release of flow after temporally clogging. Clogging is characterized by a permanent blockage of the pedestrians as shown in Fig. 4(b). In some cases lane formation

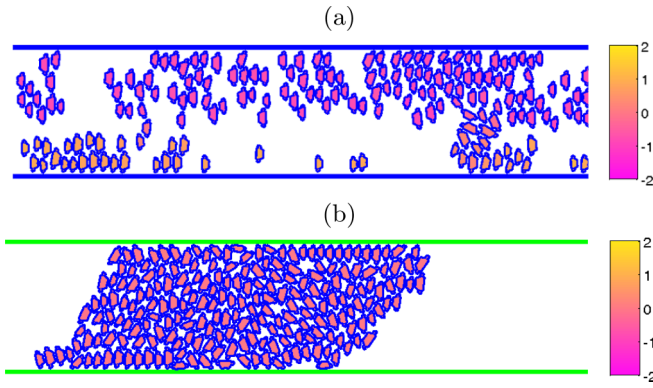


FIG. 4. (Color online) Two different regimes observed in the simulation of the hallway. (a) A snapshot of the lane formation. (b) A snapshot with the clogging. The color bar encodes the velocity in meters per second.

or clogging were observed after avalanche events. Yet we did not observe clogging after lane formation as reported by other authors [36]. This is because all forces in our model were deterministic, as opposed work from Helbing’s paper, which included stochastic forces that break lanes and induced permanent clogging.

We compared the hallway’s counterflow case with simulations of the hypothetical case of total evacuation of the venue. Evaluation of the contact forces among pedestrians gave us some insight into how the dangerous pressures built up under the crowd conditions in these two cases.

A. Simulation of the hallways

In the first series of simulations, pedestrian flow in the $3 \times 12 \text{ m}^2$ hallway was investigated with a replication of the Madrid Arena’s corridor. A random distribution of pedestrians was placed in the simulation area. Following this, a percentage of the pedestrians were assigned a desired direction towards the exit, and the others were assigned a direction towards the venue to represent the *counterflow* (the ratio between people entering and leaving the venue). With the aim to replicate observations from the Madrid Arena venue, these simulations were repeated using different densities. Periodic boundary conditions were used in the edges of the corridor. In order to demonstrate the effect of the shape of the particles in the simulation, we performed simulations where the shape of the particles were disks—their diameter is equal to our thorax shape.

Depending on the density of pedestrians and the counterflow percentage, three different regimes are observed in the simulations (see Fig. 4): (i) lane formation, which occurs at low density and is characterized by well-defined lines of pedestrian flow at the stationary stage; (ii) avalanches, which are observed at intermediate densities and counterflow values, characterized by temporal clogging of the pedestrian flow, followed by a sudden release of potential energy that leads to a short-time accelerating flow; and (iii) clogging, characterized by a frozen stage where the pedestrians are clogged indefinitely in the corridor.

An avalanche indicates that outflow in the corridor follows an intermittent flow. The time variation of the flow rate in the avalanche regime for one such occurrence is shown in

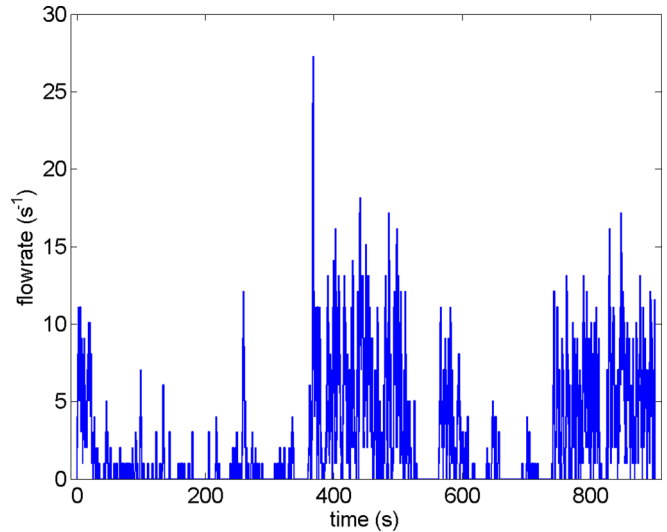


FIG. 5. (Color online) Flow-rate averaged over 1 s versus time, during a 900-s simulation on the avalanche regime. The counterflow is 75% and the density is $7.44 \text{ pedestrians/m}^2$.

Fig. 5. In this regime, the flow rate is highly intermittent, with periods of temporary clogging up to 30 s and a wide range of avalanche sizes. A major avalanche—with peak flow rate above 20 pedestrians per second—is observed in the 900 s or 15 min of simulations. This is in agreement with the video footage few hours before the tragedy, where intervals between large avalanches of 10–30 min were reported.

The existence of these three regimes allows us to represent a phase diagram of the process. Figure 6 shows the phase diagrams of these different situations using both disks and spheropolygons to represent pedestrian’s shapes. Note that the diagram is symmetric with respect to the value of the counterflow. The avalanche regime is sandwiched between the clogging and the land-formation regime. Below $4.4 \text{ pedestrians/m}^2$ and below a counterflow of 20%, the model predicts a formation of stationary lanes. The formations of avalanches without clogging appear up to a pedestrian density of $5.8 \text{ pedestrians/m}^2$ and a counterflow up to 34%. These avalanches are critical in pedestrian safety as they can produce people falling down and clogging entire hallways. The most dangerous situations are observed above $5.8 \text{ pedestrians/m}^2$ and counterflow between 34% and 66%. In these cases the model predicts complete clogging, which leads to long-lasting pressure among the pedestrians and, if the pressure is too high, possible injury by asphyxiation.

It is interesting to note that the phase diagram depends on the pedestrian shape used in the model. Thoracic particles are prone to clogging at a lower density than disks particles; in the former it suggests clogging above $3.8 \text{ pedestrians/m}^2$. Besides, the avalanches in the thorax model are less pronounced than in the model of circular particles. This is probably due to the shoulder rotation of the thoracic-shape pedestrians, which reduces the accumulation of stress that produces avalanches and eddylike motion in the boundaries between lanes. We should note that the resistance of the pedestrians to being pushed back depends on several psychological conditions and cultural background. These are accounted by the parameters

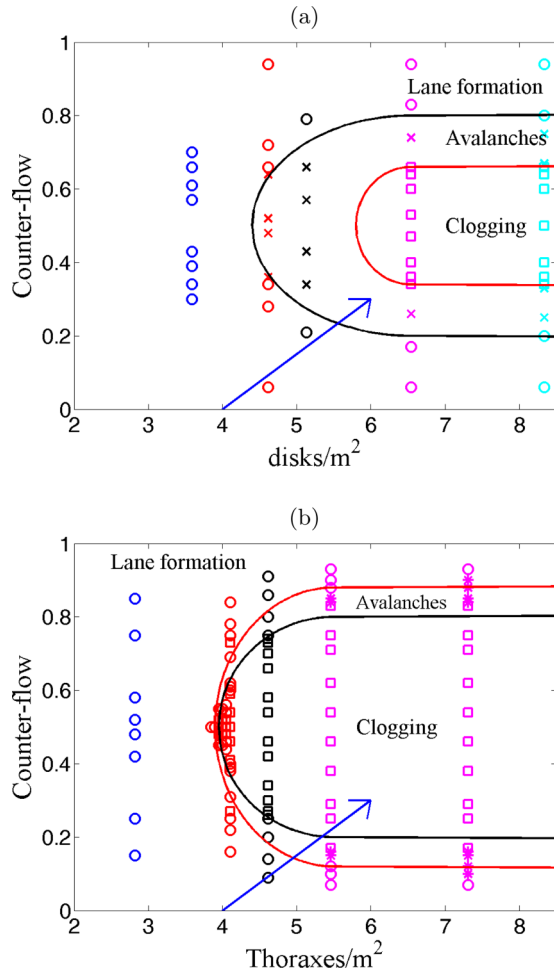


FIG. 6. (Color online) Phase diagram of the simulations of counterflow in the corridor with circles (a) and thoraxes (b). The regimes observed are lane formation (disks), avalanches (crosses), and clogging (squares). The arrow shows the time evolution of these two parameters in the hallways in the Madrid Arena. It started to form a dense crowd of people leaving the party. Then a counterflow of people joining the event increased the density, and, finally, it produced the avalanches and eventually the fatal clogging. Note that the thoraxes clog more easily than disks.

Γ_L and Γ_F of Eqs. (11) in our model, which has been fitted from comparison of simulations with video footage observations. To expand the applicability of our model to a more general circumstances, we will investigate how the phase diagram depends on these regarding pedestrian behavior parameters.

The arrows in the Fig. 6 indicate the suggested evolution of the crowd dynamics before the fatal incident in the Madrid Arena pavilion. Well before the incident, the corridor had low density (4 pedestrians/ m^2) and all pedestrians were exiting the venue (counterflow = 0%); as time passed, some people started to use the corridor to enter the venue, increasing the density and creating counterflow. The lane formation turned into dangerous avalanches that led to complete clogging in the corridor. Comparing the phase diagrams of disks and thoraxes, we note that the thorax model gives more conservative predictions of the avalanches and clogging that may lead to fatal incidents.

B. Effect of the pedestrian behavior on the crowd dynamics

With the aim of investigating the effect of the individual behavior of the pedestrians on the crowd dynamics, we performed a series of simulations using $\Gamma_F = 0.5, 1, 2$ and $\Gamma_L = 0.5, 1, 2$. For each pair of parameters, we ran simulations varying the density of pedestrians (pedestrians per square meter) and the size of the counterflow. The probability of clogging was calculated as the ratio of samples where clogging occurred divided by the total number of trials. In the same way, the probability of avalanches is obtained as the fractions of samples where avalanches were observed.

The effect of the reflex of the pedestrians to move right (Γ_L) in the probability of clogging is shown in Figs. 7 and 8. We observed that as Γ_L increased the probability of clogging decreases. This is in agreement with the intuitive idea that the cooperative behavior reduces the likely of clogging events. Something different is observed when the instinct of the pedestrians to resist moving backward as Γ_F is increased. This is shown in the Figs. 9 and 10. If Γ_F increased, the probability of jammed states in the crowd increases. This suggests that a crowd with aggressive pedestrians are more likely to produce higher instances of jamming and clogging and that a cooperative strategy results in safer outcomes.

Finally, we study the probability of avalanches as a function of the counterflow and the pedestrian's behavior parameters Γ_L and Γ_F . As Γ_L is increased the probability of having avalanches—and hence falling—increased. For the lowest Γ_L value the avalanches happened between a counterflow of 70–82% with a maximal probability of 20%. And for the highest Γ_L the avalanches are observed between counterflow of 62–82% with a probability of avalanches up to 80%. This suggests that pedestrians with strong tendency to move right are likely to produce dangerous avalanches. We presume another mechanism is used to avoid avalanches in crowds, such moving in the flow and seeking regions of lower density. This was not in the scope of our simulations and is recommended for further work. Similar results are obtained when we increase the aggressiveness parameter Γ_F . For pedestrians with low aggression, the probability of avalanches occurs between counterflow of 60–90% up to 40%. For highly aggressive pedestrian, the avalanches range narrowed to 75–90% but the probability peaks at 70%. We infer that aggressive pedestrians are more likely to produce dangerous avalanches but within a narrower range of counterflow regions than pedestrians with lower aggression (Figs. 11 and 12). Again, the psychology of the crowd seems to rule the formation of the avalanches that may eventually lead to people falling down, producing clogging in the crowd.

C. Cumulative size distribution of forces and fraction of injuries

As it was reported in the Madrid Arena incident, most of the injuries happening in dense crowds are related to asphyxiation due to high crowd pressures. There is a lack of specific data concerning this type of force in these situations that cause asphyxia by crushing. Some data are found from major crowd catastrophes such as those in Bolton in 1946 [33], Glasgow in 1971 [37], or Sheffield in 1989 [38].

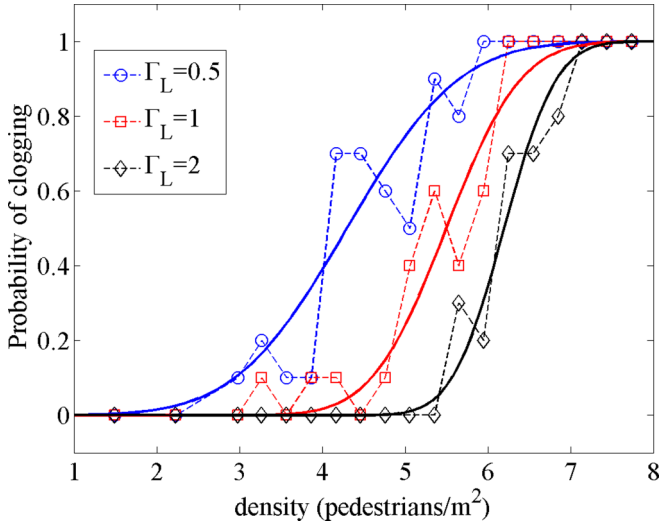


FIG. 7. (Color online) Probability of clogging versus density of pedestrians for three different values of Γ_L . The counterflow is fixed to 50%. Each symbol represents the probability calculated using 10 simulations. The continuous curve is the fit using the function $[0.5 + 0.5 \operatorname{erf}((\rho - c)/w)]$, where erf is the error function, ρ is the density, $c = 5.8, 5.3, 4.5$, and $w = 1.5, 1, 0.7$ for $\Gamma_F = 0.5, 1, 2$.

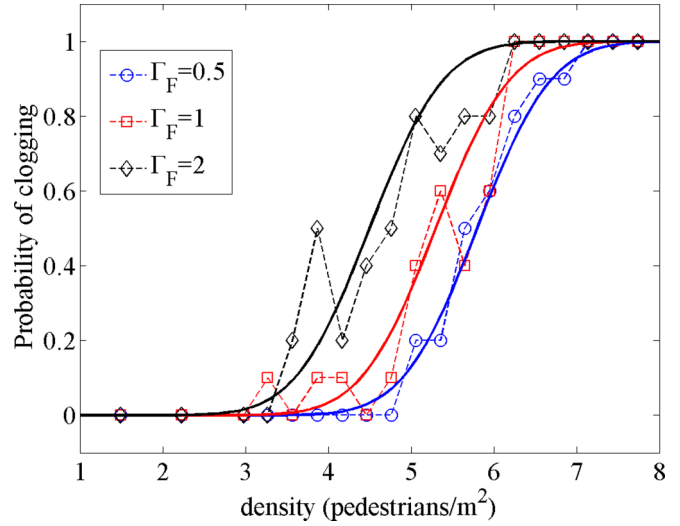


FIG. 9. (Color online) Probability of clogging versus density of pedestrians for three different values of Γ_F . The counterflow is fixed to 50%. Each symbol represents the probability calculated using 10 simulations. The continuous curve is the fit using the function $[0.5 + 0.5 \operatorname{erf}((\rho - c)/w)]$, where erf is the error function, ρ is the density, $c = 5.8, 5.3, 4.5$, and $w = 1, 1, 1$ for $\Gamma_F = 0.5, 1, 2$.

Smith and Lim [39] carried out an experimental investigation of the loads that people can stand when being pushed against a barrier. A lower-bound comfort level that could be withstood for 30 s or so without major distress was determined. Smith and Lim report on undated studies at the University of Surrey where subjects were pulled against a barrier by means of cords attached to a pack frame on the subject's back. Part of these tests attempted to measure a subjective load level of discomfort estimated by the subject to become intolerable

after a few seconds. The mean load determined at chest level from 17 subjects was 418 N with a minimum of 116 N and a maximum of 774 N. Hopkins *et al.* [40] also measured pressures in a public event. The data were collected during an 85-min performance by the English band Ride at a heavy rock concert in Britain. These crowd pressures were measured from the load measuring transducers attached on eight panels arranged in front of the stage, each of which was 1.5 m long. During the concert, people pressed against the barriers and in

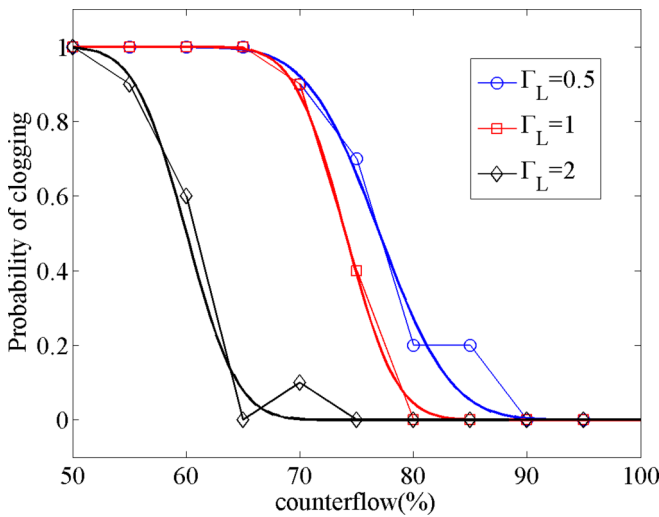


FIG. 8. (Color online) Probability of clogging versus counterflow of pedestrians for three different values of Γ_F . The density of pedestrian is fixed to $7.44 \text{ pedestrians/m}^2$. Each symbol represents the probability calculated using 10 simulations. The continuous curve is the fit using the function $[0.5 + 0.5 \operatorname{erf}((\rho - c)/w)]$, where erf is the error function, ρ is the density, $c = 77, 74, 60$, and $w = 7, 5, 5$ for $\Gamma_F = 0.5, 1, 2$.

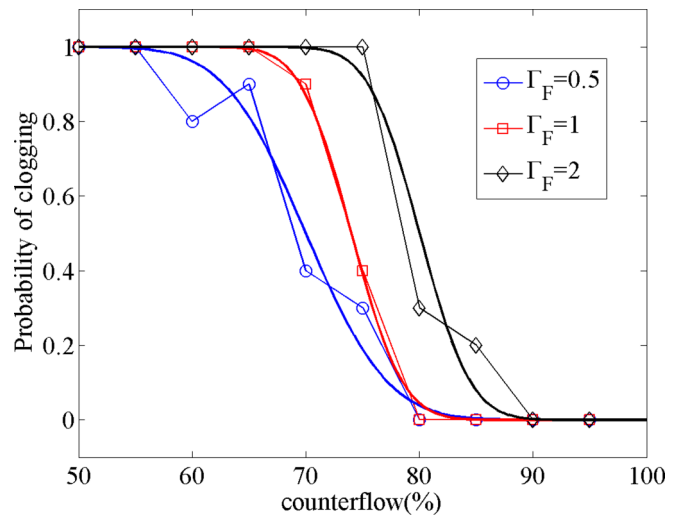


FIG. 10. (Color online) Probability of clogging versus counterflow of pedestrians for three different values of Γ_F . The density of pedestrian is fixed to $7.44 \text{ pedestrians/m}^2$. Each symbol represents the probability calculated using 10 simulations. The continuous curve is the fit using the function $[0.5 + 0.5 \operatorname{erf}((\rho - c)/w)]$, where erf is the error function, ρ is the density, $c = 70, 74, 80$, and $w = 8, 5, 5$ for $\Gamma_F = 0.5, 1, 2$.

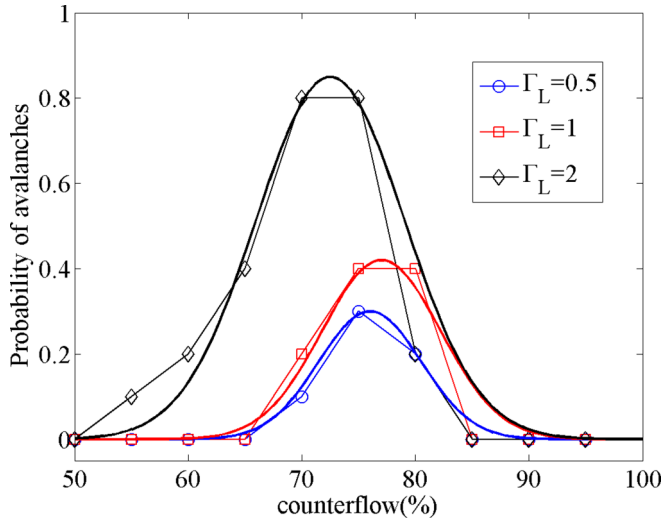


FIG. 11. (Color online) Probability avalanches versus counterflow of pedestrians for three different values of Γ_L . The density of pedestrian is fixed to 7.44 pedestrians/m². Each symbol represents the probability calculated using 10 simulations. The continuous curve is the fit using the function $h * \text{gauss}(x, w, c)$, where $\text{gauss}(x)$ a Gaussian function centered in c and with width w . The fitting parameters are $h = 0.3, 0.42, 0.85$, and $c = 76, 77, 72.5$, and $w = 4.5, 5.2, 6.5$ for $\Gamma_F = 0.5, 1, 2$.

distress were rescued by being pulled over the barriers and being treated by medical staff. Throughout the first half of the concert this outward force was sustained between 400 to 500 N.

It is difficult to assess the load and the time needed to produce asphyxia in our empirical case (the five girls at the Madrid Arena); however, taking into account the visual observation of the incident a reasonable estimation of the

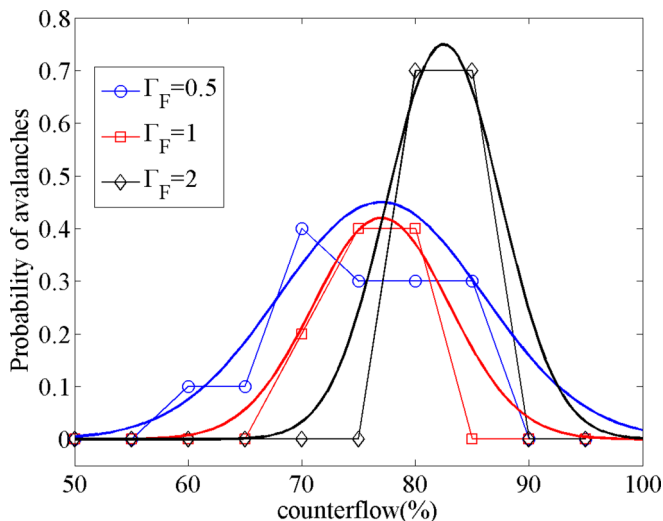


FIG. 12. (Color online) Probability of avalanches versus counterflow of pedestrians for three different values of Γ_F . The density of pedestrian is fixed to 7.44 pedestrians/m². Each symbol represents the probability calculated using 10 simulations. The continuous curve is the fit using the function $h * \text{gauss}(x, w, c)$, where $\text{gauss}(x)$ a Gaussian function centered in c and with width w . The fitting parameters are $h = 0.45, 0.42, 0.75$, and $c = 77, 77, 82.5$, and $w = 9, 6, 5$ for $\Gamma_F = 0.5, 1, 2$.

load might be 400 N, considering the number of stacked pedestrians. These data will be used in our simulations to provide estimates of the number of people at risk.

Two different cumulative size distribution scenarios were considered: the clogged hallway and the entrance in the case of panicking evacuations. Video footage from the Madrid Arena disaster showed that, after five human avalanches in the hallway, some pedestrians fell down, which subsequently created a occlusion near the exit of the corridor. To simulate this blockage some additional rules were included in the dynamics regime: If pedestrians accelerate above 5 m/s² they were assumed to fall down. A fallen pedestrian was assumed to behave like an obstacle; that is, they cannot either rotate or translate. A snapshot of the simulation of this clogging is shown in Fig. 13. The fallen pedestrians create bottleneck conditions, which lead to a stable clog. At this stage, most of the pedestrians enter into physical contact, creating a contact network. We represent this contact network by drawing a line from the center of mass of the pedestrian to the contact point and encoding the magnitude of the force by the thickness of the line.

The contact network between the particles, shown in Fig. 13 as an example, demonstrates that the forces on particles are strongly heterogeneous, as their distribution is not uniform but organized in the form of filamentary structures that granulologists call *force chains*. When applied to pedestrian motion, these force chains can determine which pedestrians suffer the largest forces and are most likely to choke. At any given point, a pedestrian may bear enormous forces, while an adjacent pedestrian may experience almost no force. In Fig. 13 we also see the percentage of pedestrians who are safe, uncomfortable, or in danger.

A dramatic distribution of contact forces is observed in the hypothetical case of an evacuation in a large room filled with pedestrians. A simulation was conducted using an evacuation of 6800 pedestrians in a room with the same dimensions of the Madrid Arena. By calculating the contact network we were able to investigate theoretically the severity of the contact forces on each pedestrian and demonstrate the number of pedestrians at severe risk. The percentage of fatalities in the total evacuation case is five times larger than in the blocked corridor. Due to the stress supported by the walls, the forces built in a hallway such as the corridor of the Madrid Arena are not large enough for many pedestrians to accumulate (in the order of 10), but, due to the large deviations in the force distribution, we would expect few fatalities. Besides, due to the large duration of this clogging in the hallways (several minutes) the strongest forces were enough to produce asphyxiation in a few pedestrians.

One way to understand why the stress is larger in open spaces than in corridors is to compare the stress distribution in the crowd with that in a silo with granular materials [41]. The self-driven force in each pedestrian is analogous to gravity experienced by the particles in the silo. In both cases the stresses increases with depth and will be saturated depending on the width of the silo (or corridor). In a narrow silo (or corridor), early saturation is expected because part of the stress is carried by the friction of the walls. In a wide silo (open space) the stress will increase with depth, taking a greater distance to saturate, producing higher pressures. In a silo the

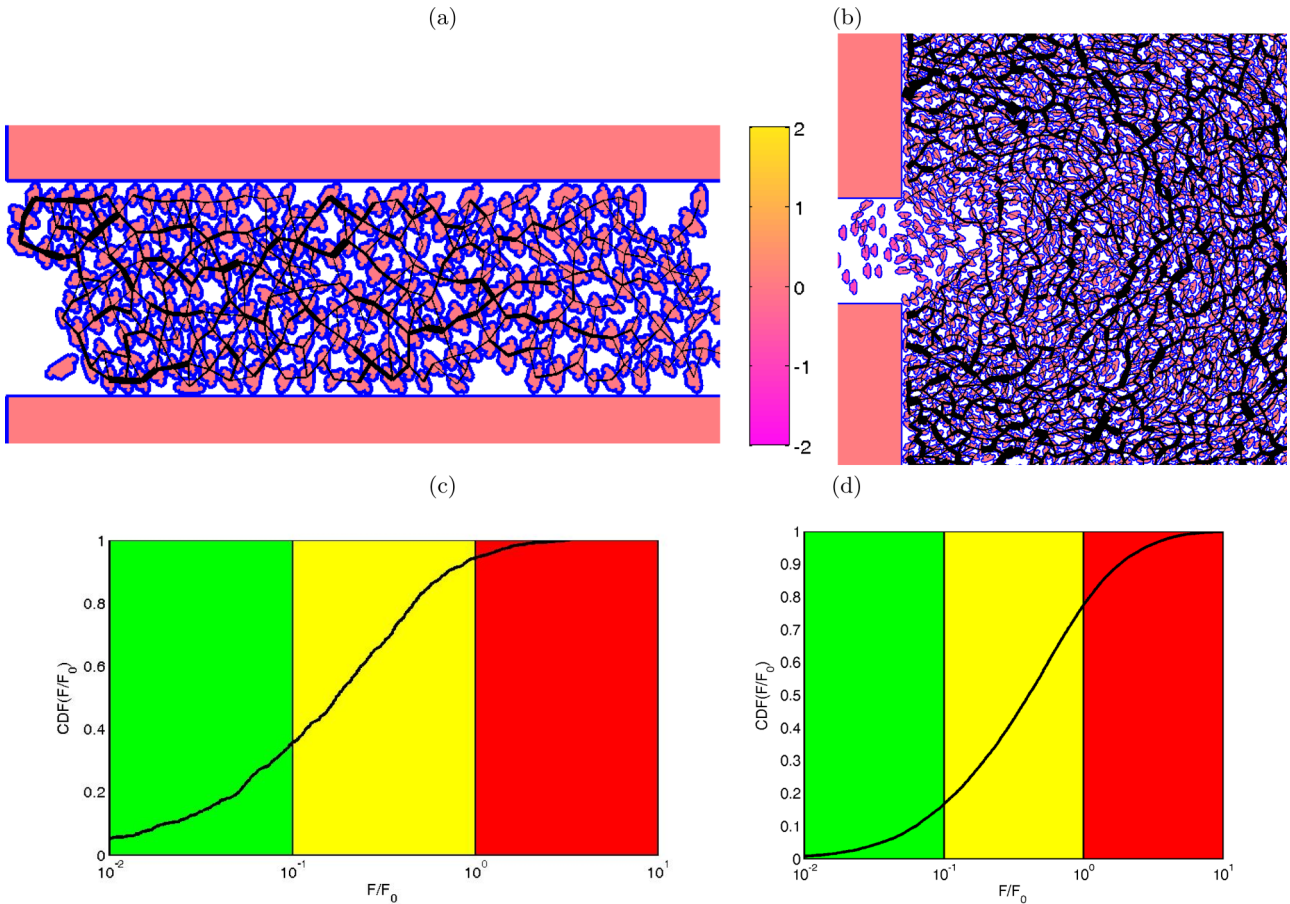


FIG. 13. (Color online) Contact-force network in the Madrid Arena. (a) The contact forces during the blockage incident in the hallway of the Madrid Arena; the thickness of the line encodes the magnitude of the contact force. The color bar encodes the velocity in meters per second. (b) shows the contact force during the total evacuation of the venue (hypothetical). (c) The cumulative distribution of forces (CDF) scaled by $F_0 = 400$ N of the case is shown in (a). (d) The CDF of this case is shown in (b). The colors in the CDF represent the safe zone (green), uncomfortable zone (yellow), and the danger zone (red).

pressure distribution is controlled by gravity and the silo’s geometry. In an human crowd in a confined space, the built-up pressure should depend on the self-driven acceleration of the pedestrians, the geometry of the exit, and the distribution of the obstacles in the space.

V. CONCLUSIONS

We presented a pedestrian interaction model based on contact forces, ground-reaction forces and torsion, and representation of thorax shapes using spheropolygons. The model is suitable for calculations of flow rates and a contact-force network under crowd conditions, where pedestrians interact more by chest and arm arrangement than by avoiding physical contact. For less dense scenarios where the private space of each pedestrian is relevant, the model may require the introduction of long-range social forces as proposed by Helbing [6]. An extended model with more developed agent decision making would allow agents to react to their local density and velocity of the crowd based on rules of herding, cooperation, and competition.

The flowability of the pedestrians in long hallways was modelled as a function of the density of pedestrians, and the percentage of pedestrians in counterflow. We obtain three regimes: lane formation, avalanched flow, and clogging. These regimes allowed us to reconstruct the incident of the Madrid Arena. From our simulations we found that the crowd in the hallway turned from a lane formation regime to an avalanche regime due to increase of density and the counterflow. These transitions suggest that the Madrid Arena incident may have been produced by an ever-increasing crowded counterflow condition that ultimately led to a fatal avalanche.

A particularly difficult aspect of the modeling was the simulation of the people falling on the floor. We have assumed that these people acted as obstacles for the other pedestrians. This is a quite crude simplification, as it simplifies a three-dimensional problem in a two-dimensional model. Yet our two-dimensional model allowed us to calculate the force experienced by the pedestrians and to estimate a small, but important, fraction of pedestrians who suffered from long-lasting pressure that resulted in asphyxiation.

Simulations showed that if total evacuation would have been implemented, it might have produced a bottleneck

situation in the entrance of the corridor. Under these conditions, our model predicts that the number of causalities would have been one order of magnitude larger. This observation is based on the force distribution in the crowd, which is similar to the stress distribution in granular piles, where the pressure increases with depth.

The force distribution found in our simulations was quite heterogeneous, suggesting that it is organizing in force chains that carry more of the load produced by the crowd. These force chains carry large forces and persist for several minutes, potentially leading to crushing and asphyxiation. It remains unclear whether an individual pedestrian could avoid being trapped by these force chains by moving their arms and rotating their chest (actually, there is an emergency procedure in these cases to help prevent asphyxia: to cross the arms with the left hand on the right shoulder and the right hand on the left shoulder.) Under dense crowd conditions, the pedestrians would have little space and would therefore find it difficult to rearrange themselves. Even if a single force chain is temporarily dissipated by a pedestrian escaping, overwhelming pressure from other pedestrians would lead to the force chain being re-established.

Two main parameters were identified in the contact-force model: the coefficient of friction, which is the main controller of the flow rate in dense granular flow, followed in importance by the coefficient of restitution. Given the

importance of these parameters it is recommended that further empirical work be conducted to provide greater model accuracy. Ethical issues can be avoided by using sand inside stitched clothes, or crash-test dummies. The test dummies would have the convenience of already having built-in sensors to measure pressure-deformation relations.

Psychological parameters that have been investigated are the Γ_L factor (related to the tendency of the pedestrians to move right to avoid collision) and the Γ_F factor (related to strength of the back force used by pedestrians to avoid being pushed back from their desired direction). These factors affect significantly the phase diagram of the counterflow dynamics. Since these parameters depend on cultural variables and special circumstances of the crowd, they would need to be calibrated by observations of crowd dynamics under similar conditions before making predictions.

ACKNOWLEDGMENTS

C.L. thanks the Asociacion de Amigos la Universidad de Navarra for support through a scholarship. F.A.M. acknowledges discussion with Iker Zuriguel, Angel Garcimartín, Chraïbi Mohcine, and Daniel Parisi and technical support from Candace Lu, Shumiao Chen, Fiona Tang Huey Ming, and Guien Miao.

-
- [1] B. D. Hankin and R. A. Wright, *Operation Research Quarterly* **9**, 81 (1958).
 - [2] W. J. Yu, R. Chen, L. Y. Dong, and S. Q. Dai, *Phys. Rev. E* **72**, 026112 (2005).
 - [3] K. Hiraki and K. Tarui, in *International Conference on Cybernetics and Society* (Institute of Electrical and Electronics Engineers, San Francisco, 1977), p. 1–778.
 - [4] R. S. C. Lee and R. L. Hughes, *Accident Analysis & Prevention* **38**, 712 (2006).
 - [5] D. Helbing, A. Johansson, and H. Z. Al-Abideen, *Phys. Rev. E* **75**, 046109 (2007).
 - [6] D. Helbing, I. Farkas, and T. Vicsek, *Nature* **407**, 487 (2000).
 - [7] M. Muramatsu and T. Nagatani, *Physica A* **275**, 281 (2000).
 - [8] C. Burstedde, K. Klauk, A. Schadschneider, and J. Zittartz, *Physica A* **295**, 507 (2001).
 - [9] D. Helbing, M. Isobe, T. Nagatani, and K. Takimoto, *Phys. Rev. E* **67**, 067101 (2003).
 - [10] D. Yanagisawa and K. Nishinari, *Phys. Rev. E* **76**, 061117 (2007).
 - [11] G. Baglietto and D. R. Parisi, *Phys. Rev. E* **83**, 056117 (2011).
 - [12] D.-M. Shi and B.-H. Wang, *Phys. Rev. E* **87**, 022802 (2013).
 - [13] S. Heliövaara, H. Ehtamo, D. Helbing, and T. Korhonen, *Phys. Rev. E* **87**, 012802 (2013).
 - [14] D. Helbing and P. Molnár, *Phys. Rev. E* **51**, 4282 (1995).
 - [15] W. G. Weng, T. Chen, H. Y. Yuan, and W. C. Fan, *Phys. Rev. E* **74**, 036102 (2006).
 - [16] D. Helbing, A. Johansson, J. Mathiesen, M. H. Jensen, and A. Hansen, *Phys. Rev. Lett.* **97**, 168001 (2006).
 - [17] D. Yanagisawa, A. Kimura, A. Tomoeda, R. Nishi, Y. Suma, K. Ohtsuka, and K. Nishinari, *Phys. Rev. E* **80**, 036110 (2009).
 - [18] C. Saloma, G. J. Perez, G. Tapang, M. Lim, and C. Palmes-Saloma, *Proc. Natl. Acad. Sci. USA* **100**, 11947 (2003).
 - [19] E. Altshuler, O. Ramos, Y. Nunez, J. Fernández, A. J. Batista-Leyva, and C. Noda, *Am. Nat.* **166**, 643 (2005).
 - [20] R. Vaughan and V. F. Hurdle, *Transport. Res. B Meth.* **26**, 381 (1992).
 - [21] K. To and P.-Y. Lai, *Phys. Rev. E* **66**, 011308 (2002).
 - [22] C. Lozano, G. Lumay, I. Zuriguel, R. C. Hidalgo, and A. Garcimartín, *Phys. Rev. Lett.* **109**, 068001 (2012).
 - [23] D. R. Parisi and C. O. Dorso, *Physica A* **385**, 343 (2007).
 - [24] I. Zuriguel, A. Janda, A. Garcimartín, C. Lozano, R. Arévalo, and D. Maza, *Phys. Rev. Lett.* **107**, 278001 (2011).
 - [25] F. Alonso-Marroquin, S. I. Azeezullah, S. A. Galindo-Torres, and L. M. Olsen-Kettle, *Phys. Rev. E* **85**, 020301 (2012).
 - [26] F. Alonso-Marroquin, *Europhys. Lett.* **83**, 14001 (2008).
 - [27] F. Alonso-Marroquin and Y. C. Wang, *Granul. Matter* **11**, 317 (2009).
 - [28] F. Alonso-Marroquin, A. Ramirez-Gomez, C. Gonzalez-Montellano, N. Balaam, D. A. H. Hanaor, E. A. Flores-Johnson, Y. Gan, S. Chen, and L. Shen, *Granul. Matter* **15**, 811 (2013).
 - [29] S. Heliövaara, T. Korhonen, S. Hostikka, and H. Ehtamo, *Building and Environment* **48**, 89 (2012).
 - [30] T. Korhonen, S. Hostikka, S. Heliövaara, and H. Ehtamo, *Pedestrian and Evacuation Dynamics 2008*, edited by C. Rogsch, W. Klingsch, A. Schadschneider, and M. Schreckenberg (Springer, Berlin, 2010), pp. 109–120.
 - [31] T. I. Lakoba, D. J. Kaup, and N. M. Finkelstein, *Simulation* **81**, 339 (2005).

- [32] P. A. Langston, R. Masling, and B. N. Asmar, *Safety Sci.* **44**, 395 (2006).
- [33] J. Busch, Master's thesis, The University of Sydney, 2011.
- [34] F. H. M. Tang, F. Alonso-Marroquin, and F. Maggi, *Water Res.* **53**, 180 (2014).
- [35] P. B. Dobrohotoff, S. I. Azeezullah, F. Maggi, and F. Alonso-Marroquin, *Granul. Matter* **14**, 651 (2012).
- [36] D. Helbing, I. J. Farkas, and T. Vicsek, *Phys. Rev. Lett.* **84**, 1240 (2000).
- [37] R. A. Smith and J. F. Dickie, *Engineering for Crowd Safety* (Elsevier, London, 1993).
- [38] R. M. Hughes, command paper 6846 (1946).
- [39] R. A. Smith and L. B. Lim, *Safety Sci.* **18**, 329 (1995).
- [40] I. H. G. Hopkins, S. J. Pountney, P. Hayes, and M. A. Sheppard, in *Engineering for Crowd Safety* (Elsevier, Amsterdam, 1993), pp. 398–398.
- [41] J. Nielsen, *Philos. Transact. Roy. Soc. London Ser. A* **336**, 2667 (1998).